

OH-stretching dynamics in trimethylamine monohydrate: What can we learn from three different direct absorption spectra?

Taija L. Fischer^a, Casper V. Jensen^b, Eaindra Lwin^a, Dhritabrata Pal^b, Henrik G. Kjaergaard^b, Martin A. Suhm^a

^a*Institute of Physical Chemistry, University of Göttingen, Tammannstr. 6, 37077 Göttingen (Germany). E-mail: msuhm@gwdg.de* ^b*Department of Chemistry, University of Copenhagen, Universitetsparken 5, Copenhagen Ø (Denmark). E-mail: hgk@chem.ku.dk*

Contents

1	Experimental Details	S3
1.1	Jet setup	S3
1.1.1	Measurement details	S3
1.1.2	Investigated compounds	S4
1.2	Matrix and room temperature gas phase setups	S4
1.2.1	Investigated compounds	S4
2	Deperturbed Uncoupled OHb Vibrational Wavenumber Estimation	S5
3	Comparison to Previous Works	S6
3.1	Experimental wavenumbers (this work)	S6
3.2	Comparison to VUV-IR and anharmonic simulations [10]	S6
3.3	Comparison to the previous argon matrix study [9]	S6
4	Spectra of Complexes of TMA and TMA-d9	S7
5	DABCO Monohydrate	S12
6	Soft Expansions as a Bridge to the Room Temperature Gas Phase	S13
7	Entries for the HyDRA Database	S13
8	Argon Expansions as a Bridge to the Matrix Isolation State	S14
9	Persistence of a gas phase combination band upon partial deuteration	S16
	References	S17

List of Tables

S1	Experimental details for the spectra	S3
S2	Investigated compounds	S4
S3	Chemical compounds for the matrix and gas phase spectra	S5
S4	Intensity centroids and their uncertainties	S5
S5	Experimental band centers from this work	S6
S6	Literature values for TMA+H ₂ O and TMA+MeOH from VUV-IR experiments	S7
S7	Literature values for TMA+H ₂ O from Ar matrix experiments	S7
S8	HyDRA database entries	S14

List of Figures

S1	Comparison of TMA and TMA-d9 with H ₂ O and MeOH	S8
S2	Dihydrate assignment for TMA	S9
S3	Comparison of TMA with MeOH for different concentrations	S10

S4	Comparison of TMA-d9 with methanol-d3 for different concentrations	S11
S5	Comparison of DABCO, TMA-d9 and TMA with H ₂ O	S12
S6	Warm expansions	S13
S7	Nanomatrix isolation	S15
S8	Gas phase combination band	S16

1 Experimental Details

1.1 Jet setup

1.1.1 Measurement details

The experimental jet data was collected by averaging # scans of gas pulses containing the compounds of interest in helium or neon through a 700 mm \times 0.2 mm slit nozzle. A Bruker VERTEX 70v FTIR spectrometer in double-sided mode at 140 kHz scanning speed with a tungsten 20 W light source, an optical filter ($<4000\text{ cm}^{-1}$) and an InSb/HgCdTe sandwich detector was used to collect the spectral data. A more detailed description of the FTIR jet setup can be found in reference [1]. Experimental details on the spectra shown in the figures (main document and supplement) can be found in table S1. The spectral traces in the range of 4000 - 2200 cm^{-1} are provided here: <https://doi.org/10.25625/IVHUHR>.

Table S1: Spectroscopic jet data used for the figures of this work (main text and supplement) including the number # of averaged scans, the date on which the spectral data was collected and the partial pressures p of the compounds/solutions. The total pressure may vary by ± 2 hPa. The TMA data shown in figure S1 is taken from figure 1 and 2 from the main document, so only the TMA-d9 data is listed. The same applies to figure S5 where only the spectrum of DABCO + H₂O is listed.

Figure 1				
$p_{\text{TMA-soln}}/\text{hPa}$	$p_{\text{H}_2\text{O}}/\text{hPa}$	p_{He}/hPa	#	dd/mm/yyyy
0.20	0.80	750	800	12/10/2023
Figure 2				
$p_{\text{TMA-soln}}/\text{hPa}$	$p_{\text{MeOH}}/\text{hPa}$	p_{He}/hPa	#	dd/mm/yyyy
0.20	0.20	750	800	13/11/2023
Figure S1				
$p_{\text{TMA-d9}}/\text{hPa}$	$p_{\text{H}_2\text{O}}/\text{hPa}$	p_{He}/hPa	#	dd/mm/yyyy
0.20	0.40	750	2000	06/11/2023
$p_{\text{TMA-d9}}/\text{hPa}$	$p_{\text{MeOH}}/\text{hPa}$	p_{He}/hPa	#	dd/mm/yyyy
0.10	0.10	750	1000	10/11/2023
Figure S2				
$p_{\text{TMA-soln}}/\text{hPa}$	$p_{\text{H}_2\text{O}}/\text{hPa}$	p_{He}/hPa	#	dd/mm/yyyy
0.20	0.80	750	800	12/10/2023
0.20	0.20	750	800	04/10/2023
Figure S3				
$p_{\text{TMA-soln}}/\text{hPa}$	$p_{\text{MeOH}}/\text{hPa}$	p_{He}/hPa	#	dd/mm/yyyy
0.20	0.20	750	800	13/11/2023
0.20	0.40	400	550	01/07/2024
Figure S4				
$p_{\text{TMA-soln}}/\text{hPa}$	$p_{\text{H}_2\text{O}}/\text{hPa}$	p_{He}/hPa	#	dd/mm/yyyy
1.00	0.00	750	800	18/10/2023
$p_{\text{TMA-d9}}/\text{hPa}$	$p_{\text{H}_2\text{O}}/\text{hPa}$	p_{He}/hPa	#	dd/mm/yyyy
0.20	0.80	750	800	07/11/2023
$p_{\text{TMA-d9}}/\text{hPa}$	$p_{\text{MeOH-d3}}/\text{hPa}$	p_{Ne}/hPa	#	dd/mm/yyyy
0.20	0.20	400	500	03/07/2024
0.20	0.70	400	800	03/07/2024
Figure S5				
$p_{\text{DABCO}}/\text{hPa}$	$p_{\text{H}_2\text{O}}/\text{hPa}$	p_{He}/hPa	#	dd/mm/yyyy
0.10	0.20	750	900	05/12/2022
Figure S6				
$p_{\text{TMA-soln}}/\text{hPa}$	$p_{\text{H}_2\text{O}}/\text{hPa}$	p_{Ne}/hPa	#	dd/mm/yyyy
5	5	10	1000	22/11/2023
0.20	0.80	750	800	12/10/2023
Figure S7				
$p_{\text{TMA-soln}}/\text{hPa}$	$p_{\text{H}_2\text{O}}/\text{hPa}$	p_{He}/hPa	#	dd/mm/yyyy
0.20	0.80	750	800	12/10/2023
$p_{\text{TMA-soln}}/\text{hPa}$	$p_{\text{H}_2\text{O}}/\text{hPa}$	p_{Ar}/hPa	#	dd/mm/yyyy
0.10	0.10	750	600	13/02/2025

1.1.2 Investigated compounds

Table S2 lists all chemicals used in the supersonic jet experiments, the code used in this work, their CAS number, supplier and purity. The strategy for TMA was to use the vapour phase above a concentrated solution in water, which initially contained mostly TMA. Therefore, mixed complexes with methanol could also be obtained from the aqueous amine solution. However, with extended use of the aqueous solution sample, the TMA concentration in the vapour phase dropped in favour of water. Therefore, table S1 only lists the combined partial pressure $p_{\text{TMA-soln}}$, which is an upper limit of p_{TMA} . For TMA-d9, a gaseous sample was used and therefore the indicated partial pressure $p_{\text{TMA-d9}}$ corresponds to that of the amine.

Table S2: Table of chemical compounds used in the supersonic jet experiments, their codes used in this work, their CAS number, their supplier and purity.

Name	Code	CAS Number	Supplier	Purity	Lot#
Trimethylamine (solution)	TMA	75-50-3	Sigma Aldrich	45w% in water	Lot-STBJ9241
Trimethylamine-d9	TMA-d9	13960-80-0	Sigma Aldrich	99 atom % D	Lot#MBBC7023
Methanol	MeOH	67-56-1	TCI	> 99.8%	Lot.NOSCB-PS
Helium	He	7440-59-7	Nippon	99.996%	
1,4-Diazabicyclo[2.2.2]octane	DABCO	280-57-9	BLDpharm	99.93%	Cat.#BD54566-5g

1.2 Matrix and room temperature gas phase setups

The matrix isolation setup combines a closed-cycle helium cryostat (CS202SI, Advance Research Systems, Inc., USA) with a Bruker VERTEX 70 FTIR spectrometer. The key details of the experimental setup are described elsewhere.[2, 3] Argon was used as the carrier gas. For the H₂O-TMA experiment, the partial pressure of H₂O, TMA, and Ar was fixed approximately to 0.93 hPa, 1.33 hPa, and 866.60 hPa, respectively. For the MeOH-TMA experiment, the partial pressure of MeOH, TMA, and Ar was fixed approximately to 0.13 hPa, 0.67 hPa, and 866.60 hPa, respectively. All the components for a particular experiment were premixed in a glass vacuum line of approximately 2.5 L. The pressures of H₂O, TMA, and MeOH were measured using an Agilent CDG-500 Series pressure gauge, and the pressure of Ar was measured using a Varian PCG-750 pressure gauge. The deposition of the gaseous mixture was carried out at 12 K on a CsI substrate using a Granville-Phillips Variable Leak valve. The deposition of the matrix was carried out for ~120 minutes at the rate of 6.88 mmol h⁻¹ and annealing was performed for about 15 minutes at 33 K. All spectra were recorded at 12 K with a SiC mid-infrared (MIR) light source, CaF₂ beamsplitter, a liquid nitrogen-cooled MCT detector, 1 cm⁻¹ resolution, and 2000 scans.

The spectrum of the room-temperature H₂O-TMA complex was taken from reference [4] and the spectrum of the room-temperature MeOH-TMA complex was taken from reference [5]. The experimental conditions and procedures are described in detail in these references but we provide a very brief summary here:

The spectrometer (Bruker VERTEX 80) was fitted with a SiC MIR lightsource and a KBr beamsplitter. Cells of 10 cm and 19 cm with KBr windows were used for the MeOH-TMA and H₂O-TMA complexes, respectively. The cells and/or vacuum glassline was fitted with Agilent CDG-500 Series pressure gauges with a full scale of 133.3 or 1333 hPa. The cell was filled with the low vapour pressure species first (H₂O or MeOH) and closed off. The pressure was measured after it has stabilized. TMA pressure was built up in the vacuum system (below 100 hPa) and throttled through the Teflon stopper into the sample cell to minimize the escaping of the low vapour pressure species.

Reference spectra of the pure compounds (MeOH and TMA) were recorded with a known pressure and the resulting spectra were subtracted with a scaling factor ~1 from the spectrum of the mixture. This leaves a spectrum of the complex only. In the case of H₂O-TMA, a spectrum of water was simulated using the software MALT [6] and the line-by-line spectrum reported in the Hitran database [7]. H₂O was subtracted leaving only small residuals. The spectrum was further refined by filtering out high-gradient points in the spectrum which arise from the non-perfect subtraction of H₂O. This yields the finished spectrum of H₂O-TMA shown in figure 1 in the main text.

1.2.1 Investigated compounds

Table S3 lists details on the chemicals used in the argon matrix and room temperature gas phase experiments.

Table S3: Chemical compounds used in the Ar matrix and room temperature experiments, their codes used in this work, their CAS number, their supplier, and purity

Name	Code	CAS Number	Supplier	Purity
Trimethylamine	TMA	75-50-3	Chemogas	>99.3%
Methanol	MeOH	67-56-1	Sigma Aldrich	99.9%
Argon	Ar	7440-37-1	Air Liquide Danmark	99.999%
Water	H ₂ O	7732-18-5	TKA Water Purification	Milli Q

2 Deperturbed Uncoupled OHb Vibrational Wavenumber Estimation

In order to estimate the centroid of the unperturbed bound water stretching vibration (OHb) in the spectra shown in figure 1 and 2 in the main document, the relevant spectral signals were integrated. This was done independently by two different people using two different strategies for integration ranges and baseline corrections, one of them including Monte Carlo noise simulation [8]. The results from the two approaches are shown together with consensus values in table S4. As the signals for the room temperature spectra are broad and partially overlapping, the integration is particularly sensitive to baseline corrections and was carried out in one step. For the low temperature measurements, the individual spectral contributions were integrated. Based on these integrals, a compromise intensity centroid with an associated uncertainty was estimated. This assumes that the IR intensity in the TMA+H₂O spectra comes only from the OHb vibration and the perturbers carry no intrinsic intensity. As the trend (shift of the centroid) from room temperature over jet to matrix conditions is similar for TMA+H₂O and TMA+MeOH, the assumption seems reasonable.

The derived centroids and their uncertainties are shown as orange bars in figure 1 and 2 in the main document and are given in table S4 for all three TMA+H₂O and TMA+MeOH spectra. Note that the Ar matrix shift of the OH centroid almost doubles from methanol to water, when attached to TMA. Although formally the difference is covered by the sum of our generous uncertainty estimates, it is quite likely significant. A possible explanation is the constraining effect of the matrix on the librational amplitude of the hydrogen-bonded OH. This constraint is larger for water than for methanol (due to mass effects on amplitude and also the better accessibility of the hydrogen bridge to the matrix atoms) and therefore removes more of the hydrogen bond-weakening perpendicular motion compared to the gas phase. In the adiabatic picture discussed in the main text (now separating fast OH stretching motion from slower OH librational motion), laterally constraining the librational effective potential in the OH-stretching ground state raises its ground state energy more than the lowest state in the more strongly bound and thus stiffer OH-stretch-excited librational effective potential. This decreases the OH stretching wavenumber (the difference between these two librational ground state energies of the complex) in the matrix, more so for water than for methanol. It is an effect qualitatively opposite to that of thermal excitation. The prediction would be that the matrix effect is even smaller for a bulky alcohol interacting with a bulky amine.

Table S4: Intensity centroids of the transitions assumed to derive intensity from OHb based on two integration approaches, the consensus value and its estimated uncertainty including baseline uncertainties and other cluster contributions for TMA+H₂O and TMA+MeOH measured at room temperature, in the jet and in an Ar matrix, all in cm⁻¹.

TMA+H₂O				
Spectral centroid (range)	Approach 1	Approach 2	Consensus	Uncertainty
room temperature centroid	3373	3372	3373	±10
(range)	(3135-3490)	(3137-3610)		
jet centroid	3300	3307	3303	±5
(range)	(3170-3390)	(3170-3390)		
Ar matrix centroid	3253	3237	3245	±10
(range)	(3150-3385)	(3160-3380)		
TMA+MeOH				
Spectral centroid (range)	Approach 1	Approach 2	Consensus	Uncertainty
room temperature centroid	3378	3372	3375	±10
(range)	(3135-3635)	(3268-3531)		
jet centroid	3308	3307	3307	±5
(range)	(3283-3332)	(3286-3331)		
Ar matrix centroid	3279	3276	3277	±10
(range)	(3237-3333)	(3240-3305)		

3 Comparison to Previous Works

3.1 Experimental wavenumbers (this work)

Band positions derived and employed in this work are summarised in table S5. They compare favourably with previous Ar matrix results [9] but are interpreted differently. They are in pronounced disagreement with previous experimental jet data [10] but agree quite well with the anharmonic predictions in that work.

Table S5: Experimental wavenumbers derived from band maxima in figures 1 (TMA+H₂O), 2 (TMA+MeOH), S1 and S2 for all three experimental techniques. At low temperature, the difference between band maxima and intensity centroids is typically small because the bands are fairly symmetric in shape. Room temperature gas phase spectra, jet cooled spectra (jet) and Ar matrix data (Ar) are compared and sorted into columns of common assignments. The values marked in color are for comparison with literature values and are further explained in the following subsections of this chapter.

room temperature	T	C	b2ON	OHb	b2
TMA+H ₂ O		3510	3331	3377	3200
TMA+MeOH				3355	
jet	T	C	b2ON	OHb	b2
TMA+H ₂ O	3487	3463	3356	3318	3195
TMA-d9+H ₂ O	3485	3456	3352	(3317/3312)	3195
TMA+MeOH				3306	
TMA-d9+MeOH				3298	
Ar	T	C	b2ON	OHb	b2
TMA+H ₂ O		3464	3359	3266	3177
TMA+MeOH		3457		3274	

3.2 Comparison to VUV-IR and anharmonic simulations [10]

In reference [10], TMA+H₂O and TMA+MeOH were investigated by a VUV-IR detection scheme and the signals were assigned using anharmonic predictions. The spectral pattern shown in [10] is very different to the one found in this work. Accordingly the assignments do not align with our interpretation. The VUV-IR experimental results and their assignments [10] are summarized in table S6. Anecdotally, the anharmonic predictions for the monohydrate [10] appear to align less well with the VUV-IR spectra than with linear spectra in this work. The predicted monohydrate OHb/b2 pair [10] is 3254/3169 cm⁻¹ and our experimental assignment is 3318/3195 cm⁻¹ (both pairs marked in orange in table S5 and S6). Also the anharmonic prediction for the combination of b2 with the intermolecular translation (ON) (3333 cm⁻¹) is close to our experimental detection (3356 cm⁻¹, both marked in red in the tables S5 and S6). The same applies for TMA+MeOH, where the anharmonic prediction for OHb is 3322 cm⁻¹ and we locate it at 3298 cm⁻¹ in the IR spectrum (highlighted in magenta in table S5 and S6).

3.3 Comparison to the previous argon matrix study [9]

In the previous Ar matrix spectrum [9] of TMA+H₂O the same signal pattern was found as in the Ar matrix data in this work. Here, the difference is in the assignment. Rather than to the TMA+H₂O 1:1 complex, the three signals are assigned to a 2:4 cluster. In the assigned structure in [9] two TMA units are connected by one water molecule, which donates a H-atom to each TMA. At the same time the connecting water molecule is part of a larger cyclic structure consisting of four water molecules. The assignment from [9] is given in table S7. The experimental wavenumbers in the table align well with the Ar matrix values found in our work, considering the width of the signals. The corresponding wavenumbers in table S5 and S7 are color coded in blue and green.

Table S6: Experimental wavenumbers $\tilde{\nu}_{\text{exp}}$, anharmonic predictions $\tilde{\nu}_{\text{ah}}$ and proposed assignments from [10]. The data for TMA+H₂O is given in the published paper [10] (table 1), while the data for TMA+MeOH is only shown in the supplement (table S1) of [10].

TMA+H₂O		
$\tilde{\nu}_{\text{exp}}$ /cm ⁻¹	$\tilde{\nu}_{\text{ah}}$ /cm ⁻¹	assignment from reference [10]
3715	3709	free OH stretch
3530	3479	coupling of water bend overtone and intermolecular translation
3462	3407	coupling among H-bonded OH stretch, water bend overtone, intermolecular translation, and intermolecular water in-plane and out-of-plane rocks
3428	3383	
3356	3333	coupling among H-bonded OH stretch, water bend overtone, and intermolecular translation
3210	3254	coupling between H-bonded OH stretch and water bend overtone
3156	3169	coupling between H-bonded OH stretch and water bend overtone
3086	3092	coupling between H-bonded OH stretch and high order excitation of intermolecular water out-of plane rock
TMA+MeOH		
$\tilde{\nu}_{\text{exp}}$ /cm ⁻¹	$\tilde{\nu}_{\text{ah}}$ /cm ⁻¹	assignment
3386	3500	The coupling between H-bonded OH stretch and intermolecular translation
3268	3322	H-bonded OH stretch
3133	3139	The coupling between OH bend overtone and intermolecular translation

Table S7: Experimental wavenumbers $\tilde{\nu}_{\text{exp}}$ in an Ar matrix from [9] (figure 1 and text) for TMA+H₂O, compared to computational predictions $\tilde{\nu}_{\text{ah}}$ in that work. We do not endorse the computational method used or guarantee correct data import.

$\tilde{\nu}_{\text{exp}}$ /cm ⁻¹	$\tilde{\nu}_{\text{ah}}$ /cm ⁻¹	assignment
3356.7	3540.6	asymmetric and symmetric stretch of a water molecule
3265.8	3489.0	in a cyclic structure donating 2 H-atoms
3176.4	-	2 δ (HOH...N)

4 Spectra of Complexes of TMA and TMA-d9

To further support the signal assignment, the hydrates and the methanolates of C-deuterated TMA were measured. This was done to confirm the robustness of the spectral pattern for the 1:1 complex, to exclude any overlap from TMA in the CH-region and to ensure that all strong signals from dihydrates and dimethanolates are visible. Figure S1 shows that the spectral pattern for the 1:1 complex is indeed robust.

To confirm that the signal marked T has a dihydrate origin, figure S2 compares two spectra with different water concentration and subtracts the lower concentration spectrum (lowest trace) from the higher concentration spectrum (uppermost trace) after scaling to similar 1:1 complex intensity (by a factor of 3). The resulting difference spectrum (center trace) only contains a single positive signal, which is attributed to a complex containing more than one water unit. Weak negative signals in the difference spectrum may point at TMA-rich clusters and combination bands of TMA itself, building on the strong CH stretching fundamentals (not shown).

In analogy to the dihydrate signal T, one can also assign a complex involving one TMA unit and two methanol units by varying expansion conditions. This is illustrated in figure S3 for regular TMA and in figure S4 for perdeuterated TMA.

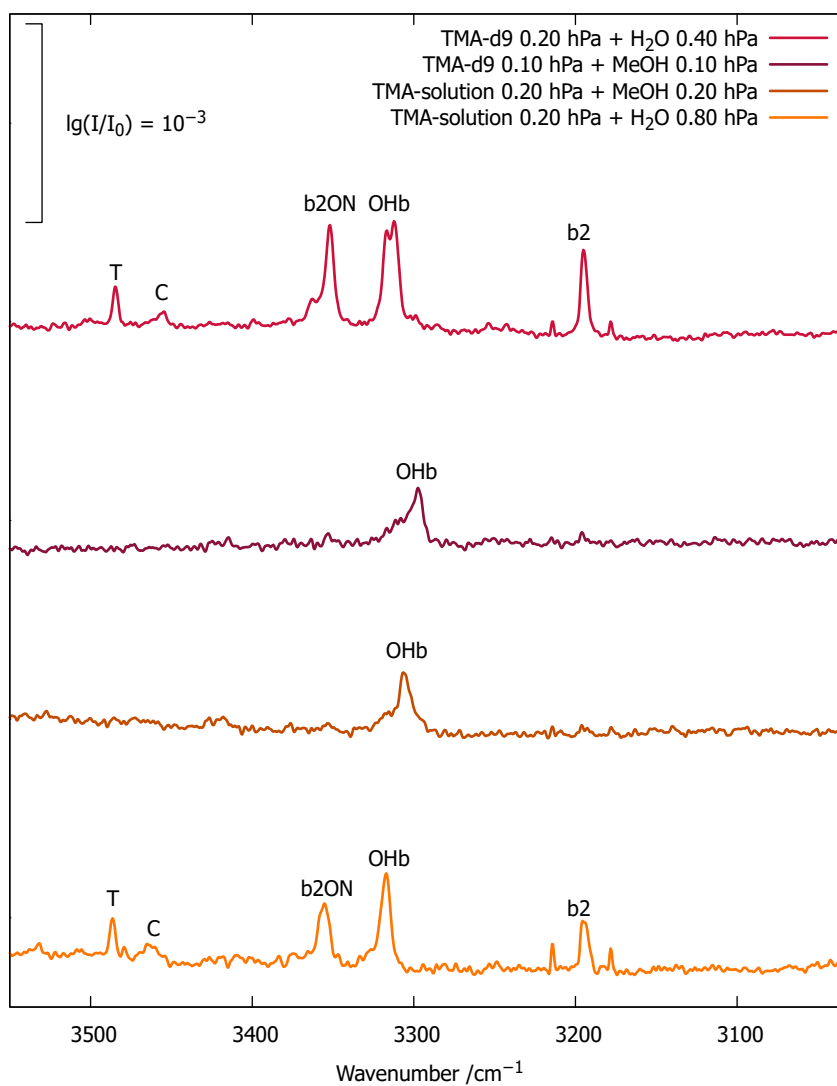


Figure S1: FTIR jet spectra of TMA (orange) and TMA-d9 (red) with H₂O (lighter tone) and MeOH (darker tone). One can see how the subtle isotope shifts do not change the spectral pattern of the 1:1 and 1:2 (T) complex significantly, whereas replacement of water by methanol consistently removes essentially all resonance partners.

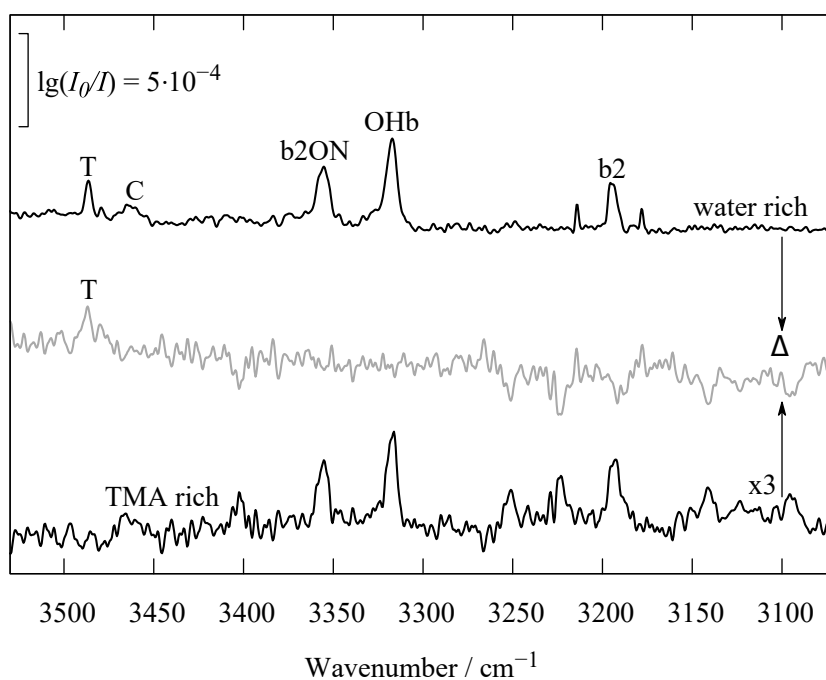


Figure S2: The dihydrate of TMA can be separated from the monohydrate features by spectral difference analysis. For this purpose, an amine-rich expansion (lower trace) is subtracted from a water-rich expansion (upper trace) after scaling the spectra such that the contributions from the 1:1 complex cancel. T as the positive difference signal in the grey difference trace is due to the hydrogen-bonded OHb signal of the water molecule coordinating the 1:1 complex as a representative of the second solvation shell (indirect amine solvation). Negative difference spectrum contributions are due to amine-rich complexes and amine combination bands building on the CH stretching fundamentals.

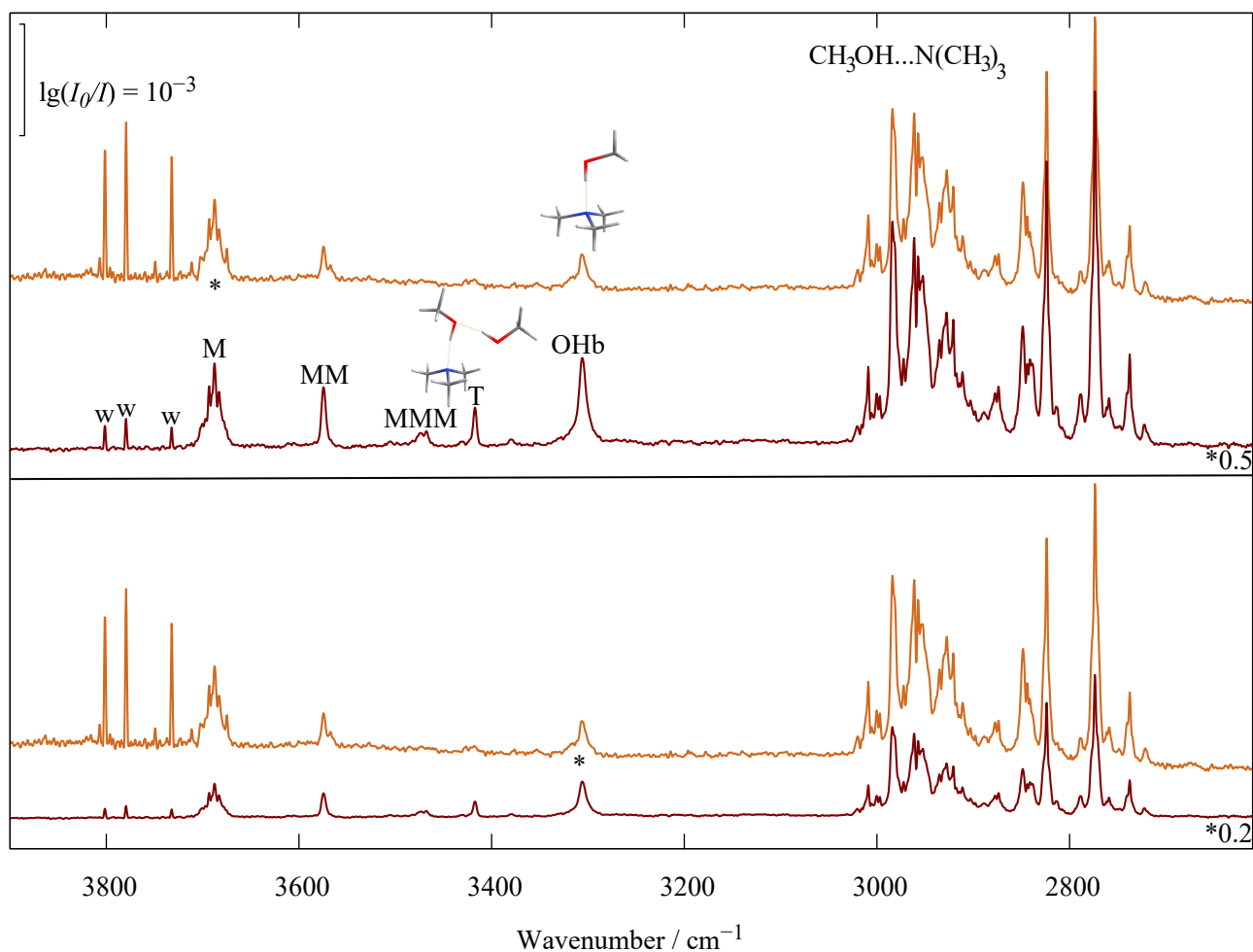


Figure S3: Comparison of the methanol/TMA coexpansion spectrum (light brown, see also main text) with a spectrum obtained at roughly twice the concentration of both methanol (M) and TMA (dark brown, containing less water (w) impurities), using two different scaling factors. With a scaling factor of 0.5 (upper pair of traces), the methanol monomer signals (M, *) becomes comparable but the mixed dimer signal (OHb) increases about two-fold, as statistically expected from the higher TMA concentration. The signal marked T increases by an order of magnitude, showing that it must contain more than one unit of methanol and/or TMA. With a scaling factor of 0.2 (lower pair of traces), the dimer signal is matched in intensity (*), whereas the signal marked T is not. This confirms the larger cluster origin of T. The signal marked MM is due to the methanol dimer and shows a similar scaling behavior as OHb. The signal marked MMM is due to methanol trimer. The CH stretching region hides other possible contributions to T, which are expected if T includes two methanol units and one TMA.

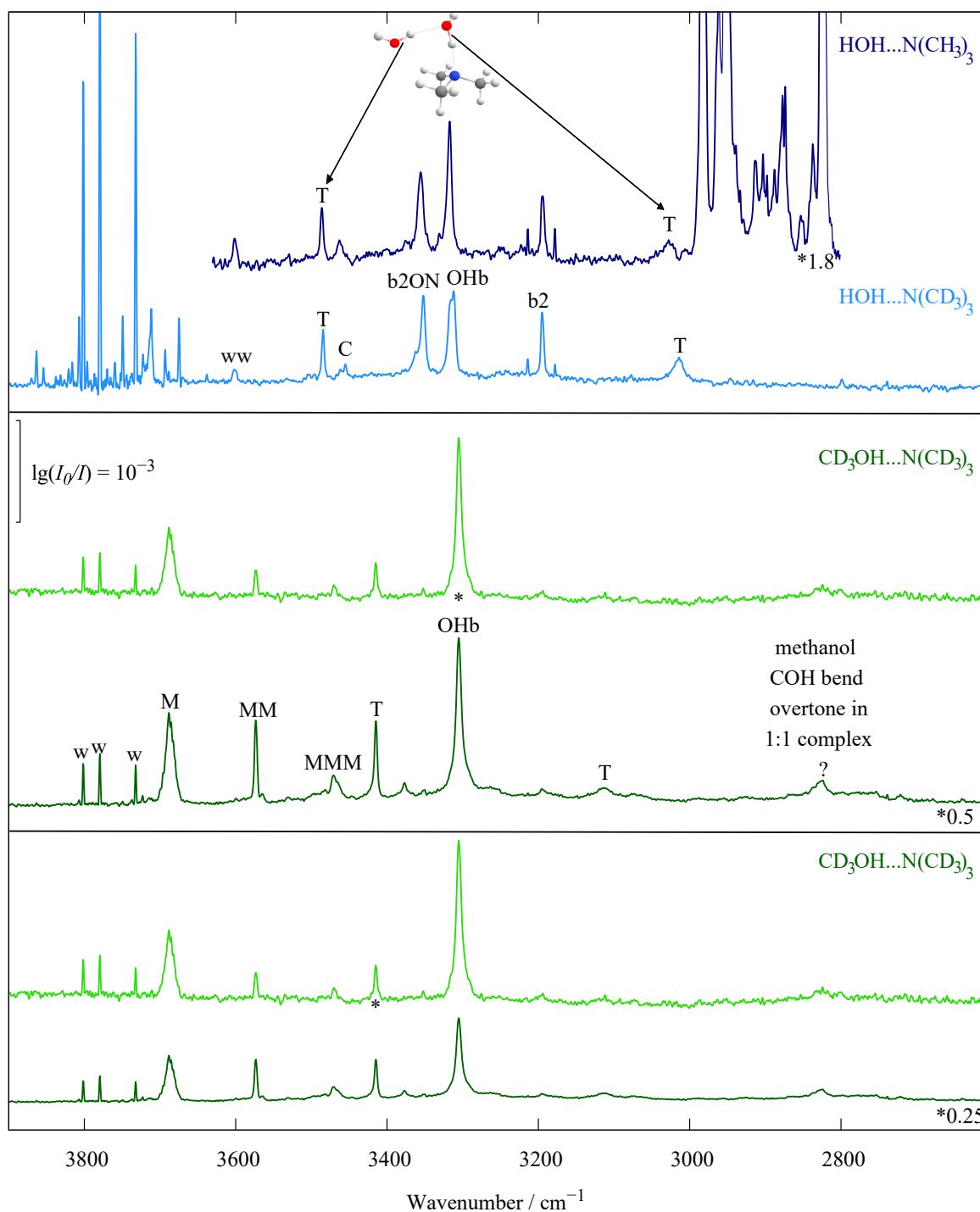


Figure S4: Comparison of fully C-deuterated coexpansion spectra with less (light green) and more methanol-d3 (dark green) and similar concentrations of TMA-d9, using two different scaling factors. With a scaling factor of 0.5 (central pair of traces), the mixed 1:1 complex signal (OHb, *) becomes comparable but the signal marked T increases significantly, showing that it must be attributed to a complex with more than one methanol-d3 unit. With a scaling factor of 0.25 (lower pair of traces), the signals marked T are matched in intensity (*), whereas the dimer signals (OHb) are not. Analogous to figure S3, the signal marked MMM shows a similar scaling behavior as T. There is evidence for further broad contributions to T in the now transparent CH stretching region, which are expected if T includes two methanol units and one amine. The methanol COH bending overtone in 1:1 complex is also visible in the lower wavenumber region around 2800 cm^{-1} . The uppermost traces combine TMA (dark blue) or TMA-d9 (light blue) with high concentrations of water to reveal not only the sharp T transition of the indirectly solvating water (OHb-i) but also the broader T transition of the water contacting the amine (OHb-c), see structure and arrows. For TMA-d9, there is only a single broad signal, for TMA a more complex pattern hidden in the CH bands cannot be ruled out.

5 DABCO Monohydrate

With DABCO (1,4-diazabicyclo[2.2.2]octane), a heavier tertiary amine was investigated in a supersonic jet expansion with water and is compared to TMA-d9 and TMA in figure S5. DABCO may be viewed as a chemical dimer of TMA, where three pairs of CH bonds are replaced by CC bonds to form a bicyclic and more rigid framework. One can see when moving from DABCO over TMA-d9 to TMA that the position of OHb is shifting slightly toward higher wavenumbers, while b2 stays at the same position and no clear trend for b2ON can be determined. Overall, the chemical substitution has effects on the water vibrations which are comparable to those of isotope substitution, providing another entry for the training of quantum chemical methods. [11]

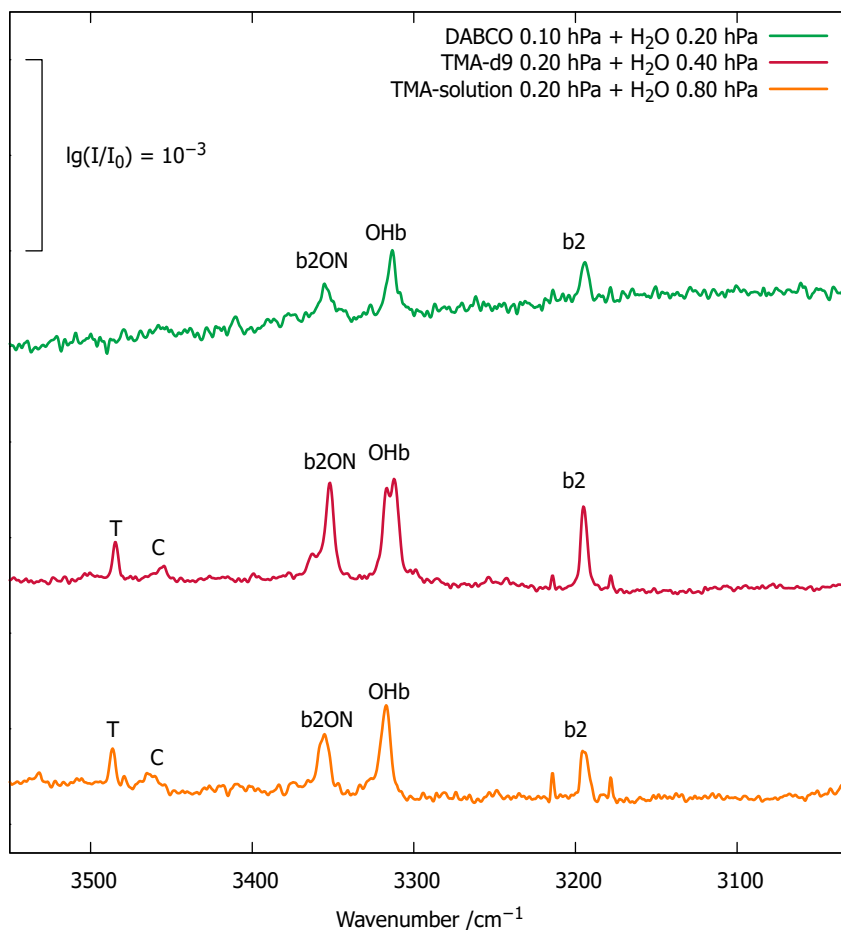


Figure S5: FTIR jet spectra of DABCO (green), TMA-d9 (red) and TMA (orange) with H₂O. One can see that the change in the band positions for the 1:1 complexes from DABCO to TMA-d9 is as subtle as the change from TMA-d9 to TMA. The higher dilution of water in the DABCO expansion suppresses the dihydrate signal (T).

6 Soft Expansions as a Bridge to the Room Temperature Gas Phase

Reduction of the stagnation pressure in a supersonic expansion allows to gradually probe warmer cluster spectra.[12] This is exemplified in figure S6, which compares the cold spectrum obtained by coexpanding about 1 hPa TMA+H₂O in 749 hPa helium (bottom) with a warm spectrum obtained by coexpanding 10 hPa TMA+H₂O in 10 hPa neon (top). One can see that amidst jet-cooled water monomer transitions and insufficiently compensated atmospheric water lines, the b2 transition loses almost all its intensity, because the OHb transition is thermally upshifted and moves away from the Fermi resonance condition. This thermal upshift also transfers intensity to b2ON and the two broad bands of similar intensity in the red spectrum are perhaps best described as $\approx 1:1$ wavefunction mixtures of stretching and b2ON dark state character. As discussed in the main text, at room temperature the two states have effectively crossed and OHb is higher in wavenumber than b2ON. Around 3100 cm⁻¹, weak combination bands building on the CH stretching fundamentals (C-H + x) appear due to the high amine content of these expansions. Dihydrates (T) do not form under these soft expansion conditions, confirming the proposed T assignment.

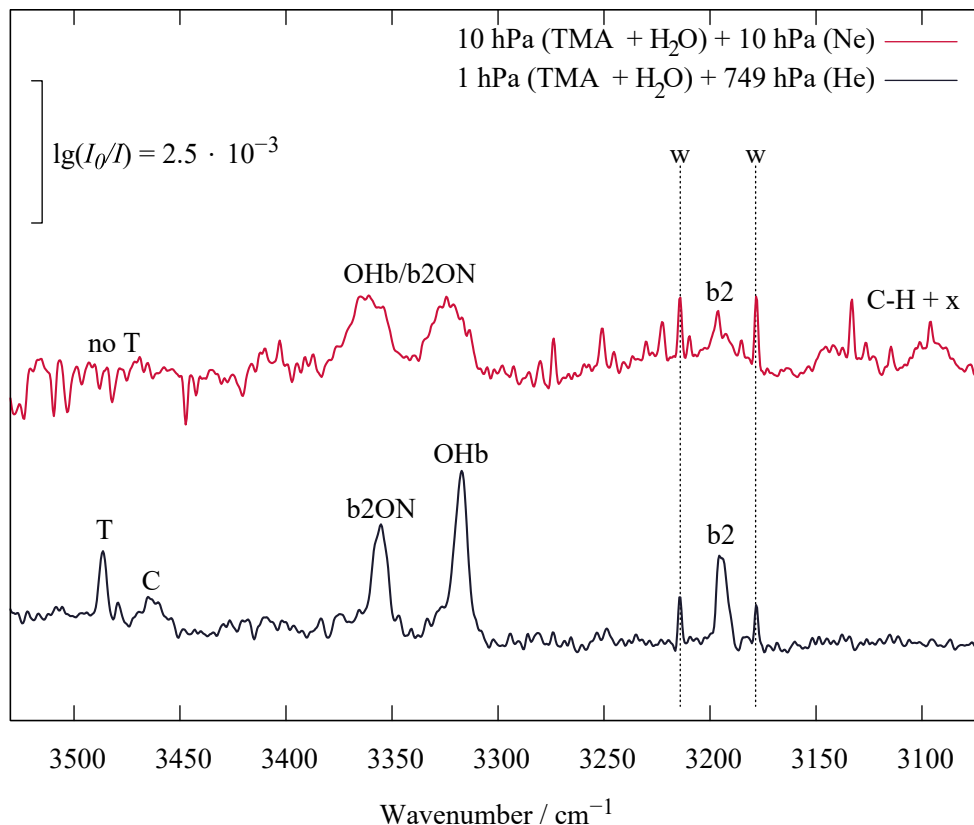


Figure S6: Comparison of a cold expansion of TMA and H₂O in He (black) to a very soft expansion in Ne (red). The thermal excitation reduces the downshift of the bright OHb state of the monohydrate due to hydrogen bond weakening, sharing less intensity with b2 and more with b2ON. Dihydrates do not form under these conditions. See text for further explanations.

7 Entries for the HyDRA Database

The supersonic jet spectra of this study can serve as references for attempts to predict hydrogen-bonded OH stretching fundamentals by theory and will therefore be included into the HyDRA database.[11] The proposed entries from this work are summarized in table S8. They include the center wavenumber of the dominant transition OHb-r (obtained as a centroid; peak positions differ from single-band intensity centroids by at most 1 cm⁻¹), the intensity fraction P of this transition among all transitions attributed to the resonance triad, the intensity centroid wavenumber OHb-d(triad) of the resonance triad which approximates the position of the OHb fundamental in the absence of resonances (assuming that the resonance partners bring in no intrinsic IR intensity and thus the appropriate target value for theoretical methods which do not treat the resonances explicitly), a final composite intensity centroid wavenumber OHb-d(final) which comprises the possibility that the weak C band also derives its intensity from OHb through wavefunction mixing and the peak wavenumber of the sharp transition T attributed to a second water molecule binding to the water molecule in the monohydrate (OHb-i, representing the second or indirect hydration shell), where available.

The OHb-d position and its uncertainty are particularly relevant for theoretical approaches which do not include

anharmonic resonances. The position is obtained as the average between the intensity centroid of the three strongest signals (OHb-d(triad), see main text) and the corresponding intensity centroid when the weak signal marked C is included. The uncertainty of this average OHb-d(final) position (in parentheses) is normally taken as the larger of the two individual centroid uncertainties. Only if this uncertainty does not span the two results with and without inclusion of C, it is increased until it does. The purpose of this conservative estimate of the deperturbed OHb position is to include the possibility that C derives all its intensity from wavefunction mixing with OHb, but also the possibility that C has its own intrinsic intensity (e.g. from vibrational Franck-Condon transitions).

Table S8: Suggested wavenumber (OHb) entries (OHb-r and OHb-d for monohydrates, OHb-i and OHb-c for dihydrates (T), in cm^{-1}) and purities of the transition closest to the intensity centroid (P , intensity fraction of the triad) for the HyDRA database derived from this work. We recommend OHb-d(final) as the target value for theoretical methods which average over anharmonic resonances. The dihydrate transitions due to water directly contacting the amine are broader and have a larger uncertainty than water in the second solvation shell.

Amine	OHb-r ^a	P	OHb-d ^b (triad)	OHb-d ^c (final)	(T) OHb-i ^d	OHb-c ^e
TMA	3319(1)	0.40-0.55	3307(3)	3315(8)	3487(2)	3027(15)
TMA-d9	3314(1)	0.40-0.50	3305(3)	3308(5)	3485(2)	3014(8)
DABCO	3313(1)	0.30-0.55	3305(6)	3311(9)		

^a raw monohydrate wavenumber (single band centroid)

^b deperturbed monohydrate wavenumber (centroid of 3 bands)

^c deperturbed monohydrate wavenumber (centroid of 3-4 bands) recommended for theory comparison

^d raw dihydrate wavenumber (peak position) for indirect solvation contact (T)

^e raw dihydrate wavenumber (peak position) for direct contact to the amine (T)

Note that while the dominant (raw) OHb-peak positions differ with isotope and chemical substitution, the uncertainty introduced by the deperturbation exceeds and thus blurs this variation. That is due to the leverage effect of the weak band C, whose intensity origin remains uncertain. Note also that the raw dominant peak position falls (nearly) into the uncertainty range of the deperturbed position, although this transition only covers about half ($P \approx 0.5$) of the triad intensity. This is due to the symmetric arrangement of the two main resonance partners above and below the OHb position.

For the dihydrate (T), we provide both the amine-contacting (OHb-c) and the indirectly solvating (OHb-i) water band positions. The latter are sharp and are therefore given a small uncertainty, whereas the former are broad, indicative of faster energy flow out of the OH stretching oscillator bound to nitrogen. For TMA-d9, we use the half-width at half maximum as the uncertainty, whereas for TMA, additional contributions underneath and distortions by the strong CH absorptions cannot be ruled out and cause a larger uncertainty.

8 Argon Expansions as a Bridge to the Matrix Isolation State

While the usual interpretation of argon matrix isolation spectra is that of substituting a few argon atoms in a more or less regular and extended lattice by the molecule or molecular complex, one can also turn the hierarchy upside down and place the argon atoms around the molecular complex in a more random way. This can be achieved in supersonic jet expansions under suitable conditions, when the helium carrier gas is replaced by argon. Depending on the stagnation pressure, the carrier gas atoms only relax the internal degrees of freedom by more efficient collisions or they start to stick on the complex and to develop solvation shells. [13] As long as these shells remain confined to the nanometre scale, it is plausible that the solvate still dictates their structure, rather than the most stable periodic solid argon ordering. Therefore, the vibrational spectra are somewhat intermediate between those of the free complex and the matrix-embedded complex. Figure S7 illustrates this for the monohydrate of TMA, by comparing the helium expansion (top), the argon expansion (middle) and the conventional argon matrix isolation spectrum (bottom trace). Vertical dashed lines mark the peak positions in the matrix and in the helium expansion. One can see that, as expected, the central OHb transition is most sensitive to the nanoshell buildup. A heterogeneous mixture of solvation environments is revealed, which spans almost the entire range from vacuum to matrix isolation. The resonance partners already reflect the matrix limit more closely, both in spectral position and spectral width, but they are still coupled to OHb and indeed one can follow how b2ON is losing IR intensity while b2 is enhanced due to the growing proximity of OHb. This is opposite to the thermal effects described in section 6. For b2, the nanomatrix absorption again falls between the vacuum and matrix isolation peak maxima. For b2ON, the effects are more subtle. The dihydrate (T) and additional monohydrate signal (C) might superimpose upon Ar addition.

Also marked in Figure S7 are negative water cluster signals [14–16] in the bulk matrix spectrum from the applied spectral difference procedure. For ww (water dimer), the Ar expansion matches the matrix value (indicating almost complete argon shell buildup in contrast to TMA monohydrate), for www (water trimer) and wwww (tetramer) there

are no counterparts in the jet expansion. Therefore, water dimer appears to be easier to converge to the bulk matrix limit than the TMA monohydrate.

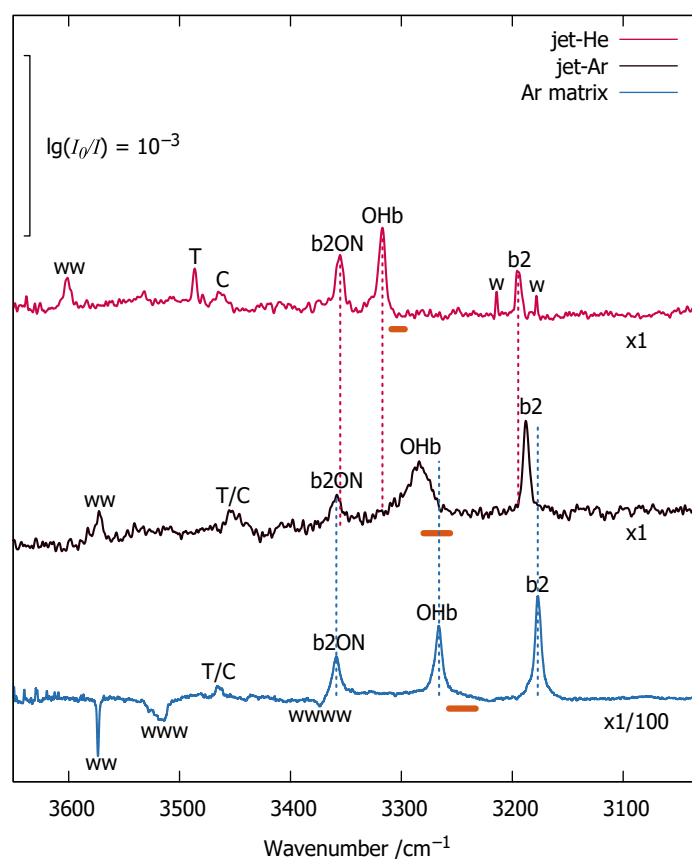


Figure S7: Spectral comparison of expansion-generated clusters between water (w) and TMA (top trace, helium as carrier gas) and matrix-isolated clusters (bottom trace) with those generated with argon as carrier gas (middle trace, partial coating of the clusters by Ar atoms creates spectral shifts). Guiding lines show how the argon expansion leads to spectral features in between those of the free and matrix-isolated reference spectra. The peak labelled OHb is particularly broad and (as the intensity centroid marked with a horizontal bar) spans almost the entire range of matrix isolation effects in its profile. See text for further explanations and Table S1 for experimental conditions .

9 Persistence of a gas phase combination band upon partial deuteration

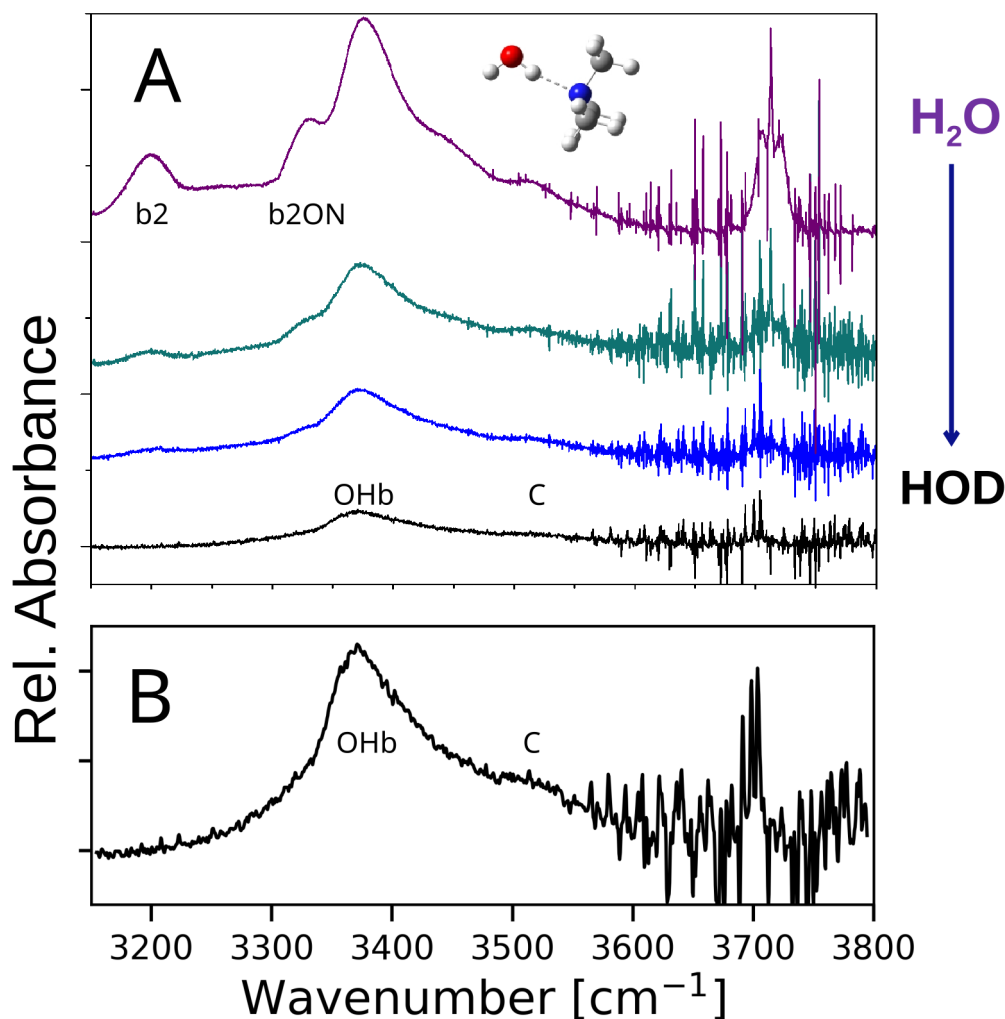


Figure S8: A) TMA monohydrate is shown with increasing deuteration of the water sample. B) A zoom of the bottom trace with maximum deuteration is shown. With increasing deuteration, the bands associated with b2 and b2ON disappear. The OH-stretching band with maximum at 3377 cm⁻¹ remains together with the "C" band with maximum around 3510 cm⁻¹. This suggests that C may be associated with the OHbON combination transition, see also Ref. [4, 5].

References

- [1] H. C. Gottschalk, T. L. Fischer, V. Meyer, R. Hildebrandt, U. Schmitt, M. A. Suhm, *Instruments* **2021**, *5*, 12.
- [2] A. S. Hansen, L. Du, H. G. Kjaergaard, *J. Phys. Chem. Lett.* **2014**, *5*, 4225–4231.
- [3] S. Li, H. G. Kjaergaard, L. Du, *J. Environ. Sci.* **2016**, *40*, 51–59.
- [4] A. Kjaersgaard, E. Vogt, A. S. Hansen, H. G. Kjaergaard, *J. Phys. Chem. A* **2020**, *124*, 7113–7122.
- [5] A. Kjaersgaard, E. Vogt, N. F. Christensen, H. G. Kjaergaard, *J. Phys. Chem. A* **2020**, *124*, 1763–1774.
- [6] D. W. T. Griffith, *Appl. Spectrosc.* **1996**, *50*.
- [7] I. Gordon, L. Rothman, R. Hargreaves, R. Hashemi, E. Karlovets, F. Skinner, E. Conway, C. Hill, R. Kochanov, Y. Tan, et al., *J. Quant. Spectrosc. Radiat. Transf.* **2022**, *277*, 107949.
- [8] N. O. B. Lüttschwager, *J. open source softw.* **2021**, *6*, 3526.
- [9] M. Rozenberg, A. Loewenschuss, C. J. Nielsen, *J. Phys. Chem. A* **2012**, *116*, 4089–4096.
- [10] S. Jiang, M. Su, S. Yang, C. Wang, Q.-R. Huang, G. Li, H. Xie, J. Yang, G. Wu, W. Zhang, et al., *J. Phys. Chem. Lett.* **2021**, *12*, 2259–2265.
- [11] Hydrate Donor Redshift Anticipation, a database maintained by the BENCH DFG research training group in Göttingen, 2024-2025, available under <https://qmbench.net/databases/hydra>.

-
- [12] E. Lwin, T. L. Fischer, M. A. Suhm, *J. Phys. Chem. Lett.* **2023**, *14*, 10194–10199.
- [13] T. N. Wassermann, P. Zielke, J. J. Lee, C. Cézard, M. A. Suhm, *J. Phys. Chem. A* **2007**, *111*, 7437–7448.
- [14] G. P. Ayers, A. D. E. Pullin, *Spectrochim. Acta Part A* **1976**, *32*, 1629–1639.
- [15] M. A. Suhm, T. Häber, *Faraday Discuss.* **2001**, *118*, 304–305.
- [16] A. Moudens, R. Georges, M. Goubet, J. Makarewicz, S. E. Lokshtanov, A. A. Vigasin, *J. Chem. Phys.* **2009**, *131*, 204312.